Absorptivity measurement of solid and powder bed under IR laser beam

Robin Kromer [a,*], Cyril Gorny [b], Elise Gruhier [c], Emilie Le Guen [a], Corinne Arvieu [a], Eric Lacoste [a]

[a] I2M-UMR 5295, University of Bordeaux, F-33400 Talence, France
[b] PIMM-UMR 8006 CNRS, Arts et métiers, ParisTech, F-75013 Paris, France
[c] I2M-UMR 5295, Arts et Métiers, ParisTech, F33400 Talence, France

Keywords:
Powder
Laser
Absorption
Density
Melting

A B S T R A C T

The effective absorptivity of IR laser light for different powder beds were studied. The reflectivity of aluminum, titanium, stainless steel and copper alloys was measured using an appropriate Ulbricht sphere. Laser irradiation was reliably detected by a photodiode. Reflectivity was carefully measured as a function of illuminated area and powder bed density. Several powder size distributions and powder thicknesses were chosen to evaluate the impact on the laser absorption. Two spot diameters were tested to evaluate the variation of the reflectivity. The absorptivity of the powder bed was significantly higher than the absorptivity of a uniform surface for similar material due to multiple scattering. In addition, the substrate is responsible for a non-negligible variation in the powder bed absorption. The inhomogeneity of the powder bed strongly modified the laser absorption for a small spot size. The absorption fluctuated during the transition from the powder state to the molten pool state.

1. Introduction

Laser powder beam fusion (LPBF) technology is one of the additive manufacturing (AM) processes that allows the fabrication of complex metal parts with high geometric accuracy. However, the LPBF process involves complex melting and solidification mechanisms and induces instabilities leading to the formation of defects that alter the final material properties [1]. Due to the complexity of laser/metal interactions, it is difficult to predict the resulting microstructure and mechanical properties [2]. Thus, many works are interested in understanding the physical phenomena induced by laser/metal interactions and by the choice of manufacturing parameters and strategies. In particular, laser/metal interactions and melt pool dynamics are strongly dependent on the energy absorbed by the powder, which in turn depends on the powder properties but also on the density and homogeneity of the powder bed [3].

The first interaction of the laser beam with the material results in the absorption of the radiation by the powder. In general, the radiation is either absorbed by the material or reflected. It has been shown numerically and experimentally that there can be significant penetration of radiation into the powder bed layer due to multi-reflections [4]. The volumetric absorption mechanism of the powder bed results in the absorption of very different amounts of energy by the material. The absorption of the material is enhanced by the fact that it is not a consolidated material. The variation in the density of the bulk material and the powder bed can explain the deviations in melting as a function of the processing strategy [5]. In addition, deviation of the powder bed density could influence the melt pool regime [6]. HaferKamp et al. [7] indicated a linear dependence of powder layer density on the average diameter of powder for monomodal powders with good flowability. This dependence can be explained by the wall effect. Fine powders with low flowability result in an increase in the standard deviation of the powder layer density. These findings suggest the existence of a particle size distribution that is sufficiently small to minimize the wall effect in a thin layer while still being sufficiently large to guarantee a good flowability of the powder. Simonds et al. [3] showed a drastic deviation of Powder Volume Fraction as one approaches the powder surface for a powder bed of thickness equal to 300 μm.

In this study, the radiation-material interaction was characterized by evaluating the absorptance, i.e., the ratio of the energy absorbed by the material to the combined incoming energy. Tolochko et al [8] and Furumoto et al [9] used an integrating sphere configuration. A frequently used laser absorption model proposed by Gusarov and Kruth [10] assumes diffusive transport of radiation in the powder. This assumption is inapplicable for the powder bed used in the LBM because of the speed of the treatment. Indeed, the energy is typically absorbed in the upper layer and this absorption is extremely non-uniform. In addition, Ali et al. [11] naturally concluded that due to the interaction

* Corresponding author.
E-mail address: robin.kromer@u-bordeaux.fr (R. Kromer).

https://doi.org/10.1016/j.optlastec.2022.108508

between the recoater and the variation in the powder bed volume accumulated ahead of the recoater across the build compartment, the relative powder-bed compaction density decreases along the recoater shifting direction (from 66.4 % to 52.4 %.). This possible variation in the powder-bed compaction density affects the density and surface roughness of the final printed parts that is also investigated. Results show that the part density and surface quality decrease −0.25 % and −20 %, respectively, along the build bed in direction of the recoater motion. This paper will investigate a similar development and propose for several materials a quantitative value of absorption during laser-powder interaction.

A cautious approach was defined to perform absorptance measurements of the powder bed layer during laser-matter interaction. The suitability of the measurement system was demonstrated by correlation with current data. Initial and final state reflectivities of the material were critically evaluated at room temperature and in an inert environment. By setting the powder bed in motion, it was possible to approach the conditions of the LBM process in a very short time. A direct comparison and discussion is proposed based on the obtained experimental results and using the density and projected area measurements.

2. Experimental procedure

2.1. Materials

2.1.1. Raw material

Six materials were selected as reference materials for the experiments. The first one is a type 316L stainless steel used as substrate, the next 3 are aluminum alloys (AlSi7Mg0.6, AlSi10Mg and AlCu), the fifth one is a TA6V alloy and the sixth one is copper. They were selected for their different applications in the industry. Two polishing states were chosen (after polishing papers P400 and P4000 - Ra: 8.6 ± 1.2 μm and 2.3 ± 0.8 μm respectively).

2.1.2. Powders

The metal powders were obtained by gas atomization (as in the LBM process) of the following alloys: AlSi7Mg0.6, AlSi10Mg, AlCu, TA6V and copper. Observations of the powders were made with a SEM (HITACHI tm3000) (Fig. 1). The aluminum alloy powders were ellipsoidal. TA6V and Cu powders showed perfect spherical shape of particles. An analysis of the powder size distribution was performed using a Mastersizer 3000 laser granulometer (Malvern). The AlSi10Mg powder distributions were divided into three batches (Fig. 2). The different materials and batches showed classically shaped powder size distributions. Table 1 describes the powder size distributions for each of the powders.

2.2. Design and experimental setup

Layering system was designed with a hopper system and flexible recoater blade. The parallelism was calibrated using a thickness gauge on different points. The recoater was mounted on a rail. A Yb:YAG (1.03 μm) was used for laser-matter interaction (Trumpf TruDisk 10000). The laser power was set to 320 W in continuous mode through a 0.2 mm optical fiber. Laser had a Gaussian shape source. A square impulsion was generated. Different square pulses from 5 to 200 ms were used. Two spot sizes were chosen: 2 mm and 0.2 mm in diameter. A density filter of 2 was used for the 0.2 mm laser beam (laser energy deposition divided by 100).

There are several methods for measuring the absorptance of a material. Indirect reflection based method, often referred to as the integrating method (Ulbricht method), is used in this study. It homogenizes the total diffuse reflection and possibly the specular reflection. The integrating sphere method asks for references with a known absorptance for the calibration of the sphere/sensor combination. A mirror (silvered on fused silica) with a reflectivity of 98.8 % (±0.2 %) was chosen for the laser wavelength. In addition, proof measurements were performed for sensor linearity and sphere uniformity with respect to beam diameter and laser power. Sphere uniformity was verified by rotating the mirror approximately 20° to check for intensity variation. Each set of measurements consisted of three laser hits. The beam power was constant with a standard error of less than 0.2 %. The integrating sphere has an internal diameter of 150 mm and contains three holes (Fig. 3). One is a laser beam entrance hole (diameter: 20 mm), another is a sample hole (diameter: 20 mm) and the third is a circular detector hole (diameter: 5 mm). The total area of the access holes was 2–3 % of the integrating sphere. The detector hole contains a threaded SM1 attachment for mounting the photodiode. The integrating sphere is equipped with a FND-100 photodiode with a measurement range of 600–1150 nm (spectral response center at 1000 nm and response time of 1 ns) and a detection area of 5 mm^2.

The integrating sphere was placed under a laser welding head. The sample holder was placed under a linear system (guided roller) for dynamic analysis. The target sample was placed at the focal plane and at a defocused distance of 200 mm. Custom samples were machined to a 3 × 3 mm surface with a thickness of 50, 100, 150, 200 and 300 μm (±3.2 μm).

2.3. Absorption analysis

The study was performed for two beam flux densities (energy per unit area). The beam output level was synchronized with the integrating sphere sensor (triggering). Measurements were made using an oscilloscope with a sampling rate of 100 kHz. The sample was cleaned between each measurement with alcohol. The tests were performed under an Argon atmosphere (<180 PPM O2).

Data were analyzed by an automated pulse detection algorithm that uses a second output (laser on/off) and a thresholding algorithm. The data points in the integrating sphere were averaged and additional statistical information (median, standard deviation) was calculated. The sensor measured the back signal intensity from the powder bed. The signal intensity was proportional to the average reflection intensity. For each measurement, the signal intensity at the very first instant was

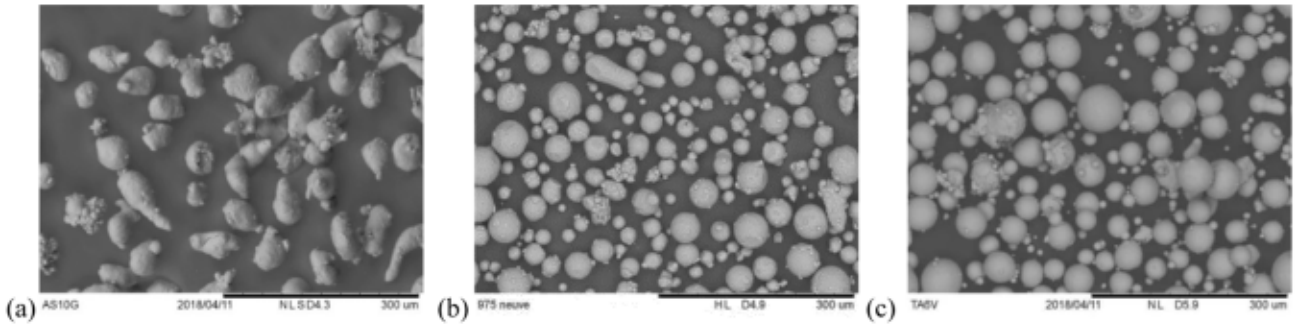

Fig. 1. Examples of free-powder observations: a) AS10G, b) AS7G0.6 and c) TA6V.

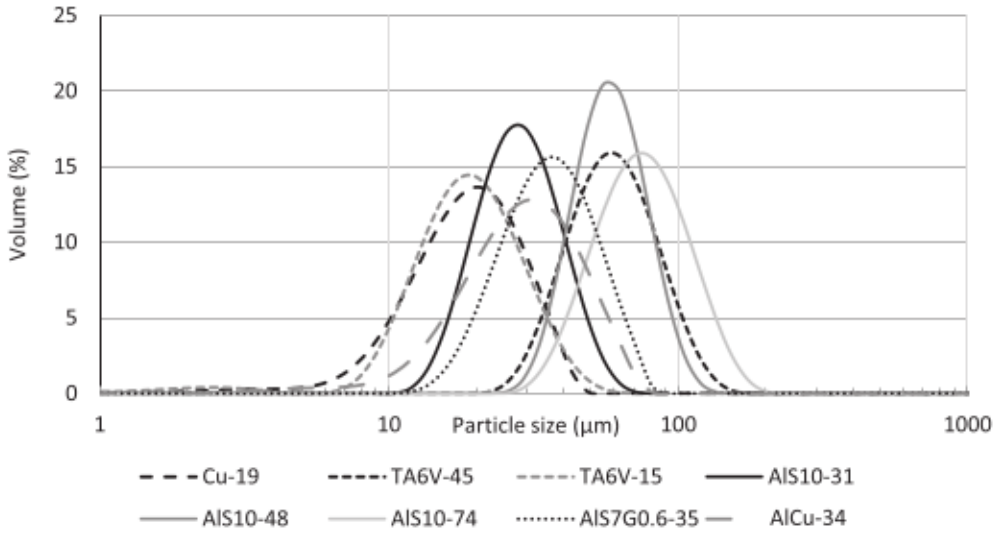

Fig. 2. Granulometry distribution of the different powders.

Table 1
Powder Size Distribution made by laser granulometer (D10, D50, D90 : log-normal distribution - means that 10% of the sample is smaller than X µm, 50% is smaller than X µm, and 90% is smaller than X µm).

Powder	D10 (µm)	D50 (µm)	D90 (µm)
Cu-19	**9,8**	**18,7**	**31,1**
TA6V-45	**28,6**	**44,9**	**87,3**
TA6V-15	**6,5**	**15,0**	**36,0**
AS10-31	**17,2**	**30,9**	**52,0**
AlS10-48	**133,7**	**47,9**	**73,7**
AlS10-74	**46,2**	**73,9**	**118,0**
AlS7G0.6-35	**21,5**	**35,3**	**56,3**
AlCu-34	**17,2**	**33,9**	**58,2**

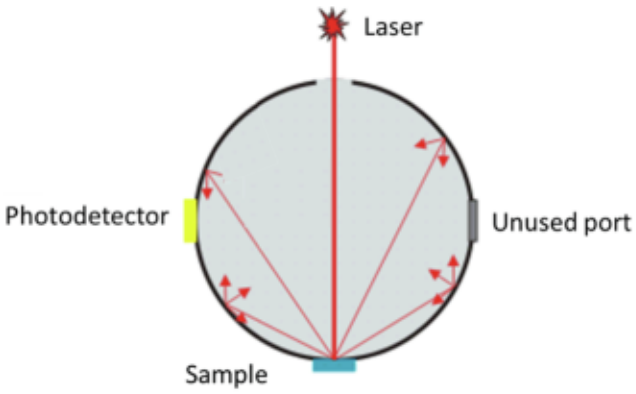

Fig. 3. Integrating sphere for absorptivity measurement.

calculated as the average over 100 data points, namely during the first 1 ms. The reflectance of the sample was calculated by comparing the sample signal to the signal of a reference material with known reflectance (mirror). The assumption of no transmission of radiation through the sample was retained because the contribution of emitted radiation was negligible (sensor threshold in the IRA wavelength). Standard deviations of reflectivity measurement is an average of the dynamic data below 5 ms for powder state or continuously for transition measurements from 5 to 60 ms (using five samples).

2.4. Powder bed layer analysis

2.4.1. Powder bed density

The powder bed layers were characterized using mass and volume measurements. Grooved supports were used to obtain specific thicknesses of the powder bed. The volumes of the square grooves were measured with a micrometer (Mitutoyo). The powders were layered eight times in the grooves and mass measurements were performed (Aczet Cy-85c balance). The density of the powder bed was calculated based on these measurements. The objective was to obtain the density of the powder bed for the different grooved substrates and powder batches.

2.4.2. Powder apparent and tapped densities

The bulk densities were measured for the different powders. The measurement method was as follows: the powders were first simply deposited and then in a second step a mechanical tapping (50 times) was performed using an extension cylinder [12]. The powder contained in the volume was weighed and divided by the volume of the cup to obtain the bulk density. Each measurement was repeated five times.

2.4.3. Projected surface analysis

The powder bed layers were also analyzed to assess the top surface interacting directly with the laser. The major challenge is the problem of ray tracing in an assembly of thousands of objects using a laser absorption model. The ray tracing capability was developed by Boley et al [4]. Calculations show that the absorptivity of the resulting powder bed is significant in the top layer of the array. Only 1 % penetrates below the second layer. The multiple scattering can be related to the total absorbing surface. Twelve surfaces were therefore constructed and analyzed by optical microscopy (VHX 5000, Keyence). The analysis of each surface was done in three steps: an area was first selected according to the diameter of the laser beam, the projected area was then calculated and then the absorptive surface ratio was deduced [13].

3. Results

3.1. Powder bed density

The density of the powder bed was measured after deposition and tapping 50 times (Table 2). The spherical particles impose a void space between them that contributes to about 50 % of the accumulated space after deposition. Repetitive tapping increased the density of the powder bed with the reduction of the adjacent free inter-connection.

Fig. 4 shows the bulk density of the powder bed layer deposited on a

Table 2
Density properties of powders (±1%).

	D50	Bulk density (g. cm^{-3})	Deposited density (g. cm^{-3})	Tapped density (g. cm^{-3})
AS10G	86	2,68	1,23	1,58
	58	2,68	1,29	1,63
	42	2,68	1,47	1,66
AS7G06	39	2,66	1,25	1,68
AlCu	37	2,68	1,13	1,74
TA6V	45	4,43	2,22	2,75
	15	4,43	2,53	2,97
Cu	28	8,92	3,92	4,91

stainless steel substrate for different powder thicknesses. These results demonstrated the effect of layer thickness and powder sizes/shapes. First, fairly consistent values are observed for layer thicknesses between 100 and 300 μm, regardless of material. These values are comparable to the average between the deposited and tapped density values. A drop in bulk density is observed when the thickness is equal to 50 μm, whatever the material. This phenomenon can be explained by sliding effects due to the force of the blade on the powder bed. Mindt et al [14] have numerically demonstrated the effect of the thickness of the powder layer on the packing density.

Secondly, this effect of falling density of the powder bed is accentuated by the size distribution of the powder: it was indeed more difficult to compact the larger size particles. For example, AS10G-72 μm powders were less compact than AS10G-31 μm powders. The cumulative gap depended on the contact force of the particles. Roller compaction was suggested. This decreased the difference in tapped density between batches of different particle sizes. Jacob et al [15] carefully studied the effect of distribution on void formation. In addition, Haferkamp et al. [7] present results that indicate that (i) the bulk density of a single powder layer is significantly lower than that obtained when there are multiple layers and (ii) fines powders result in higher powder layer densities.

Third, the shape of the particles also influences the void filling mechanisms. For example, TA6V-45 μm powders and AS10G-48 μm powders are spherical and irregular, respectively. The bulk density was more critical for the smoother particles. The compression involved by the recoater allowed the smooth particles to fill the void.

In conclusion, the interaction of particles depends not only on their shape but also on the materials. The study must therefore be performed for each powder batch configuration (size, shape, distribution) and each material. Is a direct correlation possible with the absorptivity of the powder bed under laser irradiation?

3.2. *Illuminated area ratio*

The powder beds were illuminated with two spot diameters (2 mm and 0.2 mm) with similar energy. The objective was to obtain a quantitative value of the light projected onto the particles. The illuminated area ratio is defined as the top surface (sum of the surfaces of the particles and cavities who receive the light beam) area divided by the equivalent planar area [13]. Fig. 5 shows the illuminated area ratio for 2 mm and 0.2 mm spots as a function of powders and powder bed thickness assessed by confocal microscopy.

We first notice that whatever the powder batch, the illuminated area ratio is larger with the smaller spot size. The powder bed layer could be described with convex zones (particle) and concave area (vacant space). If we place ourselves in the 2 limiting cases, the photon flux can interact on 2–3 particles when we have a large powder size distribution and a small spot size, or on 300–500 particles when we have a small powder size distribution and a large spot size. So, we have a very different illuminated area depending on the configuration. So, illuminated area are directly link to the cumulative photon number hitting particle top or side. Light hitting the sides of powder particles will reflect much more strongly than light hitting the top. Therefore, from the point of view of light scattering, illuminated area ratio is hence used to compare more easily the reflectivity values for the discussion.

For the small spot, significant deviations on the ratio of the illuminated surface is observed because of the inhomogeneity of the powder bed. These deviations are quite small for the larger powder thicknesses (150 μm, 200 μm and 300 μm) and more pronounced for the smaller thicknesses (100 μm and 50 μm). These differences can be explained by the mechanical interaction between the particles and by the passage of the blade which leads to a segregation of the powder bed layer.

These results show that the density of the powder bed was not homogeneous. Fig. 6 shows two examples of surface analysis after powder

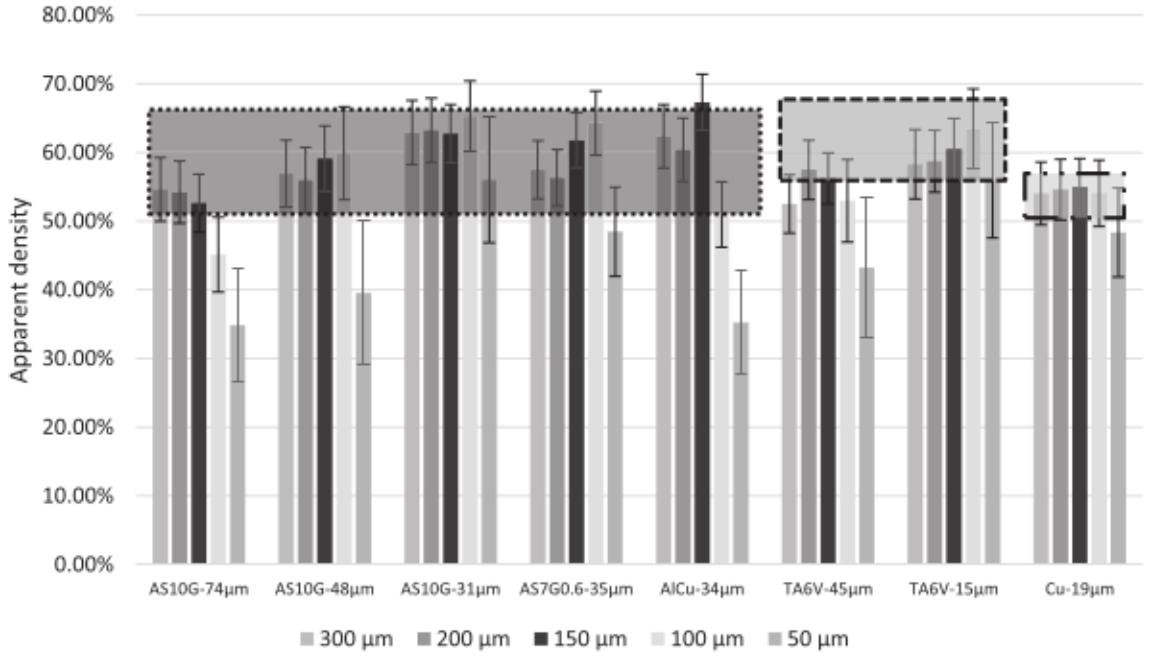

Fig. 4. Apparent density of powder bed layer from 50 to 300 μm on stainless steel and deposit and tapped density threshold (bottom and top respectively) represented by dotted rectangles.

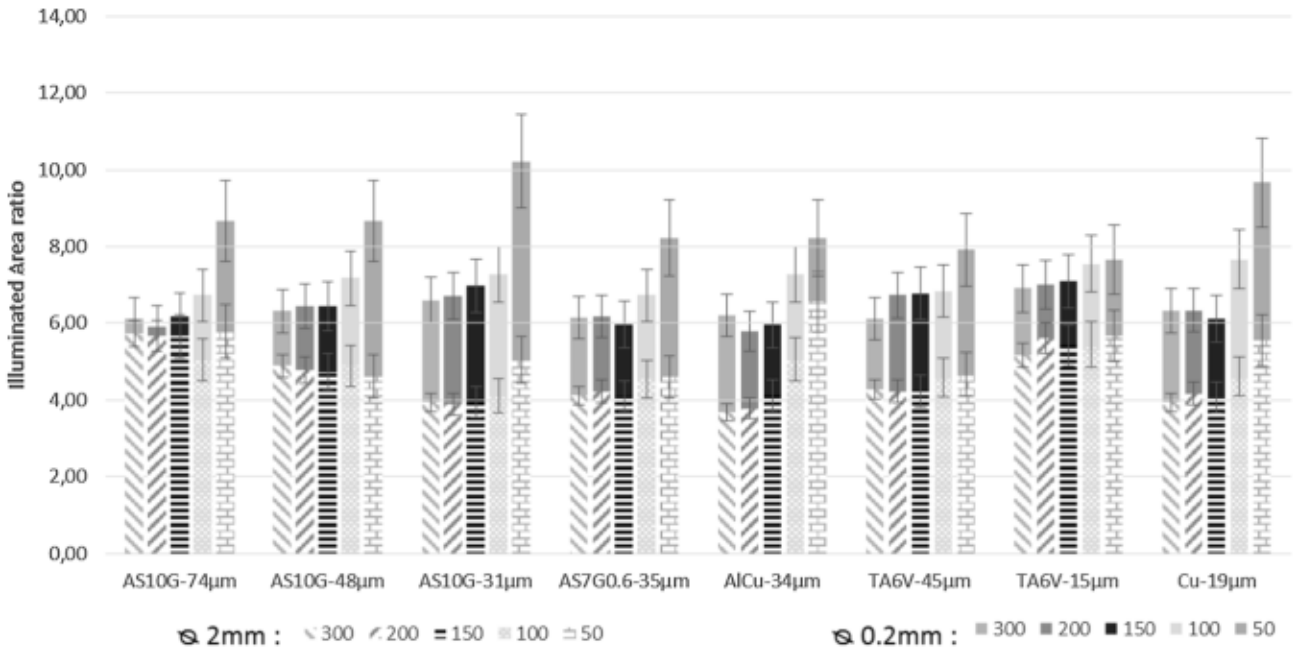

Fig. 5. Illuminated area ratio for the different materials and different thickness from 50 to 300 µm - hatched: ⌀2 mm and solid: ⌀0.2 mm.

stratification (voids are highlighted in blue). A relatively good layering can be observed for the thickness of 100 µm (Fig. 6a). On the contrary, with a thickness of 50 µm one can observe a compact block with the presence of voids (Fig. 6b). The circles indicate the different stripes.

Finally, the standard deviations (for 8 analyses) of the evaluated illuminated areas were close to 7 % and 10 % for powder thicknesses ranging from 100 to 300 µm and close to 11 % and 15 % with a thickness of 50 µm, for spots of 2 mm and 0.2 mm respectively.

Even if the errors on the results (Figs. 4 and 5) are important, it was shown that the density of the powder bed and the illuminated surface vary according to the materials, the batches of powders and the thicknesses of powders (for a fixed geometry and speed of the recoater).

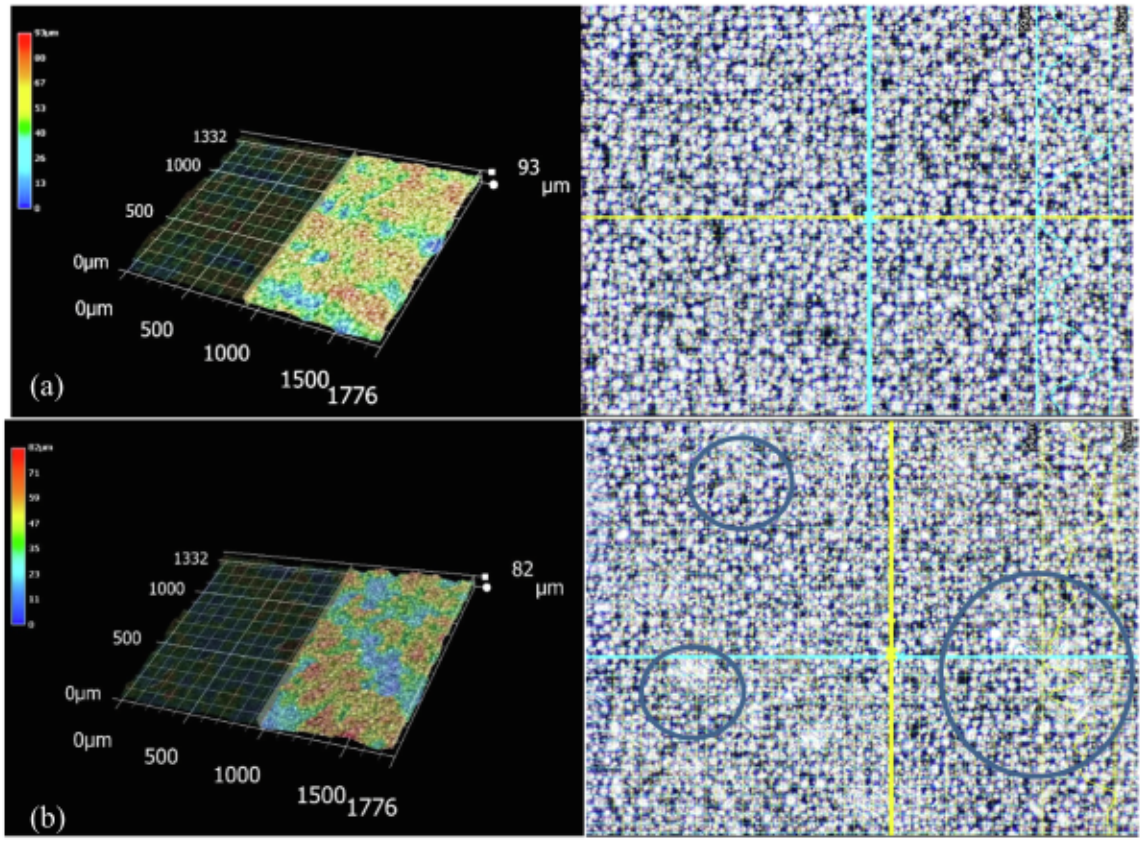

Fig. 6. Top-view and surface analysis of titanium particles - (a) 100 µm and (2) 50 µm depth.

3.3. Raw substrate absorption

An Ulbricht sphere was used to evaluate the absorptivity. Fig. 7 represents the measurements for different reference materials obtained with 2 polished surfaces (P400 and P4000) and with the 2 laser spot sizes (2 mm and 0.2 mm diameter).

The results observed for raw stainless steel were consistent with the values reported for unpolished stainless steel (35–50 %) [16]. The other materials were compared to the work of Boley et al [17] who proposed a modeling of the interaction using a ray tracing calculation: the values obtained for a flat surface of Al, Ti, Cu and Stainless Steel were respectively 4.7, 39, 2.8 and 34 %. Their values were quite similar to those obtained with a P4000 for each material.

Although silicon and copper contents slightly influenced the absorptivity, the results obtained with different aluminum alloys show that the material composition has little influence on the reflectivity. On the other hand, the roughness has a more important impact: the absorptivity increases of approximately 30 % when the surface is polished. Thus, we observe that the illuminated surface evolves from 1.08 ± 0.56 to 1.48 ± 0.47 when going from a rough surface (P400) to a polished surface (P4000) respectively. A P400 polished surface was used for powder bed evaluation. A value of 40 % is then highlighted on Figs. 8 and 9 to show the substrate reference.

Note that the standard deviation in Figs. 7, 8, and 9 represents the average values below 1 ms that are associated with the powder state using 100 points for each of the 5 samples.

3.4. Powder bed absorption evaluation

Powder beds, ranging in thickness from 50 to 300 μm, were deposited on the substrates. Initially, the reflectivity was measured for dissimilar materials and powders with a 2 mm spot size. Fig. 8 shows the absorptivity obtained for the different configurations as well as the average absorptivity value of the stainless steel (substrate).

The absorptivity measurements showed a direct influence of the material and the size of the powders. Aluminum alloys have values varying around 53–63 %, except for AlCu powder which has a lower value estimated at 36 %. Titanium alloy has the highest values, around 60 %. As expected, copper had almost no absorptivity at the IR wavelength.

A decay of absorptivity for the largest powder size distributions (AS10G-74 μm and TA6V-45 μm) was noticed from a powder thickness of 100 μm. This phenomenon can be explained by the volumetric laser-matter interaction due to a multi-diffusion phenomenon [4].

The absorptivity of the powder bed was significantly higher than the normal incidence value on a bulk (polished surfaces). This effect was also observed by Tolochko et al [8]. Multiple scattering was responsible for the additional absorption compared to the case of a uniform surface. Thus, the relative increase in absorptivity was higher for highly reflective metals (Al) than for moderately absorbing metals (Ti). In the former case, the ratio (powder bed absorptivity divided by polished substrate absorptivity) ranged from 4.5 to 7.2, while in the latter case, the ratio decreased to about 1.7.

To approximate the spot diameters used in additive manufacturing, a spot size of 0.2 mm was therefore investigated to provide a qualitative picture of absorbed irradiance on a short time scale compared to thermo-mechanical times (Fig. 9). A decrease in absorptivity of the order of 10 % is observed compared to the initial 2 mm spot, regardless of the configuration. The absorptivity is thus sensitive to the beam size. It has been observed by Boley et al [17] that the fluctuation becomes negligible for a beam radius greater than four times the particle diameter.

3.5. Absorptivity evolution

Absorbance measurement using a 0.2 mm spot was recorded for 100 ms for three different materials: AS10G, TA6V and Cu (Fig. 10). Note that the highlighted area in Fig. 10 represents the average standard deviation measurement using 100 points for each of the 5 samples. The gray area defined the previous absorptivity results. Several samples were stopped after 5–10-20–50-100 ms for observation. During the first times, the reflectivity of the powder bed was measured to obtain the sintering state after about 1 ms. During this stage, whatever the material, the absorptivity increases due to the approach of the particles between them. From 1 to 5 ms for AS10G and Cu or from 1 to 20 ms for TA6V, it was noticed a phenomenon of stable sintered state of the material which can be associated with the constant absorptivity (red zone in the Fig. 10). Then, the powder remains in the sintered state even if the temperature increases. This zone is defined as a phase transition (in blue on Fig. 10). During this step, for AS10G and TA6V, the absorptivity decreases due to the compaction of the powder. For Cu, we do not observe any multi-scattering effect due to the proximity with the liquid state. Finally, the layer started to melt (bubble) from 10 to 50 ms depending on the material. From these observations, three states at different times of the laser-matter interaction are clearly evident. We have plotted on Fig. 11 the observations for the AS10G at different times which correspond at the different zone observed in the Fig. 10: in the

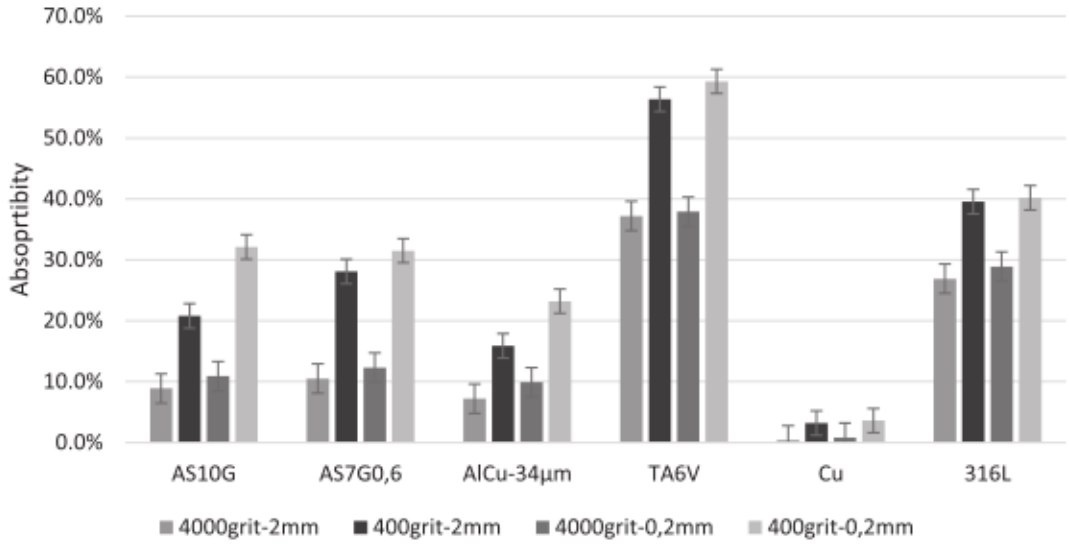

Fig. 7. Average absorptance measurement for several materials – polished 4000grit and rough 400grit.

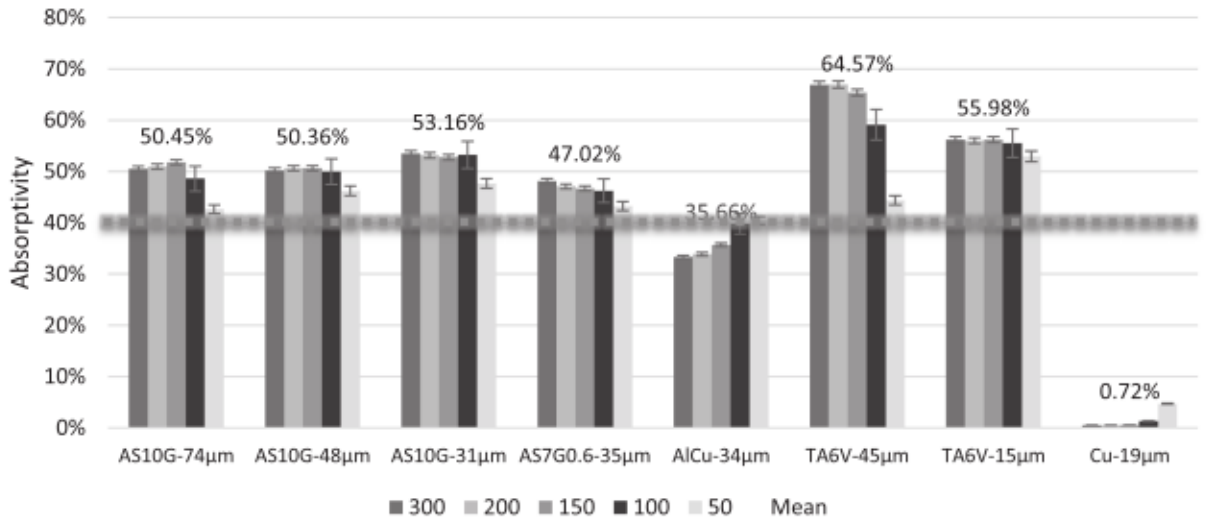

Fig. 8. Average absorptance measurements for several powders and material for ⌀2 mm - powder bed layer thickness from 50 to 300 µm - highlighted values: mean – line: absorptivity of the substrate.

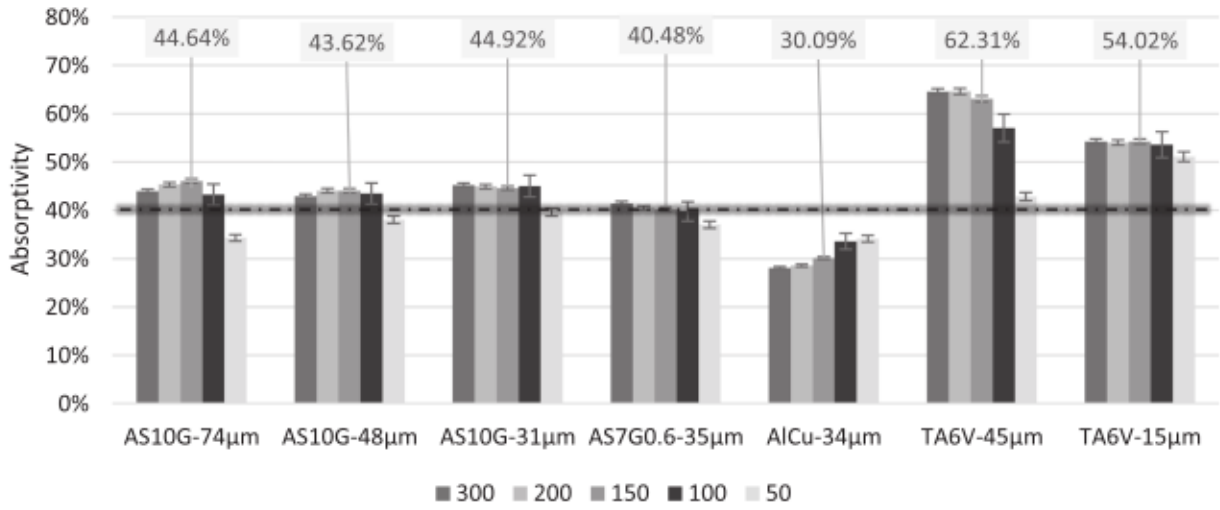

Fig. 9. Average absorptance measurements for several powders and material for ⌀ 0.2 mm - powder bed layer thickness from 50 to 300 µm - highlighted values: mean – line: absorptivity of the substrate.

Fig. 11 a and b material is in the sintered state while it is in the liquid state on the Fig. 11c. Finally, we could observe that for some materials (Ti and Cu), a sphere started to form because of the surface tensions.

Aluminum and titanium alloys had a similar behavior. The values increased due to particle sintering phenomena, then stabilized and decreased as the temperature increased. For copper, particle sintering and phase transition significantly changed the interaction. The liquid phase increased strongly absorption. Dependencies with temperature were suggested and will be discussed.

3.6. Dynamic measurements

Absorbance measurements were also studied with kinematics. The sample was moved at 500 mm/s, which is representative of the interaction between the laser power and the powder bed during additive manufacturing processes, even though the energy density was limited and the laser spot slightly larger. The powder bed remained in the solid state after the experimental tests. A slight sintering phenomenon was observed. Fig. 12 shows the absorptivity for TA6V and AS10G for a 0.2 mm spot size. The straight lines represent the average values previously observed in the static configuration, with the associated standard deviation whose limits are represented by 2 horizontal lines.

A fluctuation was observed during the laser-matter interaction. The variations were close to the standard deviation obtained for the absorptivity measurements. However, it was noticed that there were different areas where the values crossed the limits of the standard deviation. Therefore, the absorptivity could be dependent on the density of the powder bed and/or the illumination area. This will be discussed in more detail.

4. Discussion

The absorption and deposition of energy in a metal powder bed has been studied experimentally. A discussion in 2 parts is proposed: comparison with the literature for the different materials and effect of multiple scattering phenomena on the absorbed energy.

4.1. Comparison Bulk – Powder – Liquid

Several papers have evaluated the reflectivity of materials with laser interaction, but they are not specifically associated with the development of additive manufacturing. Bulk materials have often been studied.

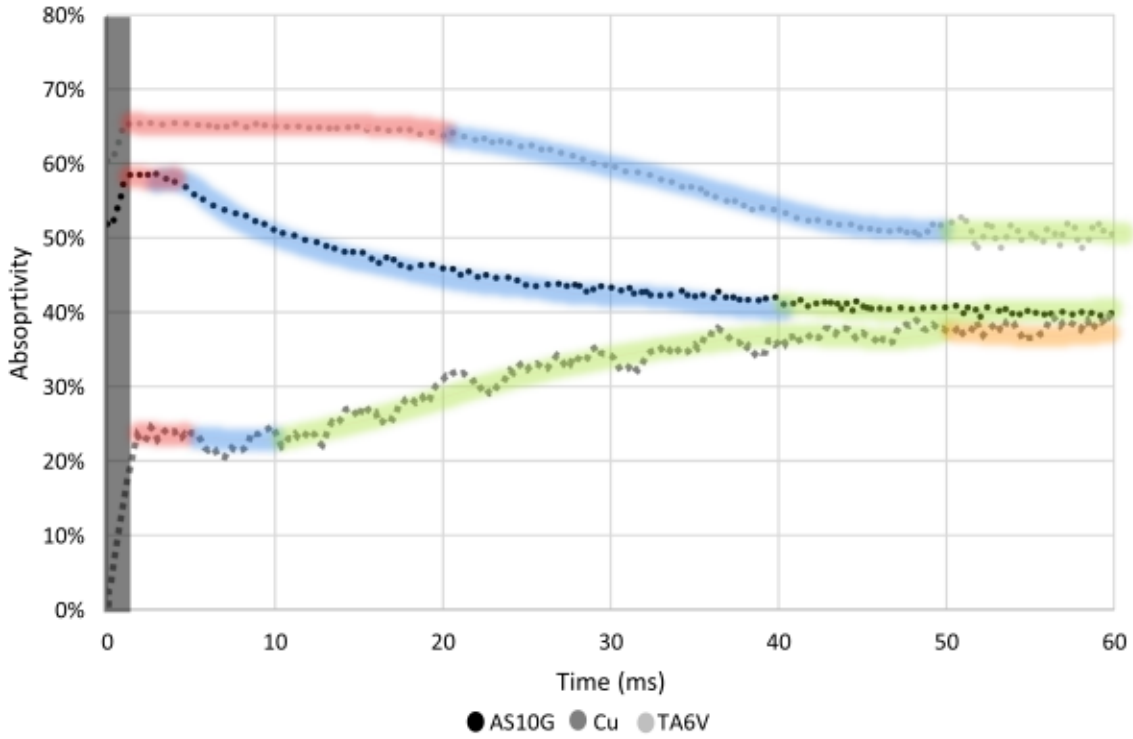

Fig. 10. Absorptivity of AS10G-48 μm, TA6V-45 μm and Cu with a 100 μm powder layer – highlight: solid / red: sintering / blue: phase transition / green: liquid (disk shape) / orange: liquid (sphere shape). (For interpretation of the references to colour in this figure legend, the reader is referred to the web version of this article.)

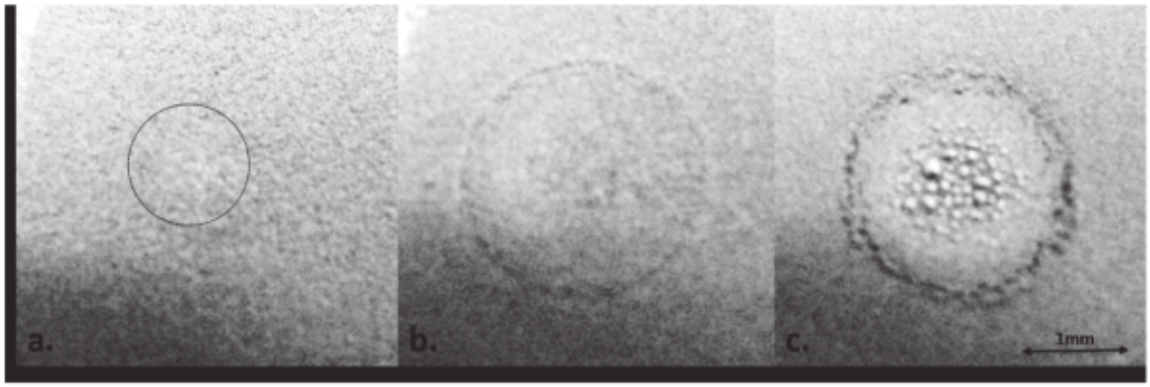

Fig. 11. Top-view after laser interaction for AS10G-46 μm after a. 5 ms, b. 20 ms, c. 50 ms.

Liquid phases have also been considered in the laser welding process. The absorptivity of the liquid phase for 2 and 0.2 mm spots was studied using measurements after 150 ms. Indeed, at this time, the material is in its liquid phase as we have shown previously (Fig. 10). This liquid phase can be considered as an ideal candidate to verify the methodology (Fig. 13). The reflectivity of the bulk material has already been presented (Fig. 7).

According to the studies of Bergström et al [16], the reflectivity was equal to 20 %, 5 % and 40 % for aluminum alloy, copper and stainless steel respectively. These values were similar for large and small laser spots for P400 surfaces, meaning that our values are relevant. It is clear that roughness can influence the reflectivity due to a larger interaction area. Furthermore, it was also noted that the absorptance changes in the liquid phase. The laser-matter interaction was associated with electron vibration. The liquid allowed more freedom compared to the structured crystalline solid phase. The values observed for the evolution of Cu absorptivity are comparable to those obtained by the work of Chen et al. [18] Gunenthiram et al [19] reported the same evolution between the solid and liquid states for 316L stainless steel. Other papers used the CO2 laser and thus the results are not comparable.

However, the values may also vary depending on the substrate, the powder deposition system, and the laser interaction strategy. In-situ control of temperature and absorptivity is needed to go further and evaluation of powder bed density needs to be developed.

4.2. Absorbed energy

The impacts of spot size and powder bed thickness on absorptivity were observed. In addition, a variation of the density of the powder bed was highlighted. The laser-matter interaction was thus complex and multifactorial. The evaluation of the absorbed energy showed a decrease for strongly absorbing materials and an increase for strongly reflecting materials for smaller powder thicknesses. The absorption ratio of the substrate was indeed considerable. A volume ratio between the absorptivity of the powder and the substrate due to multi-diffusion is necessary. The support of the powder bed must also be evaluated (peaks,

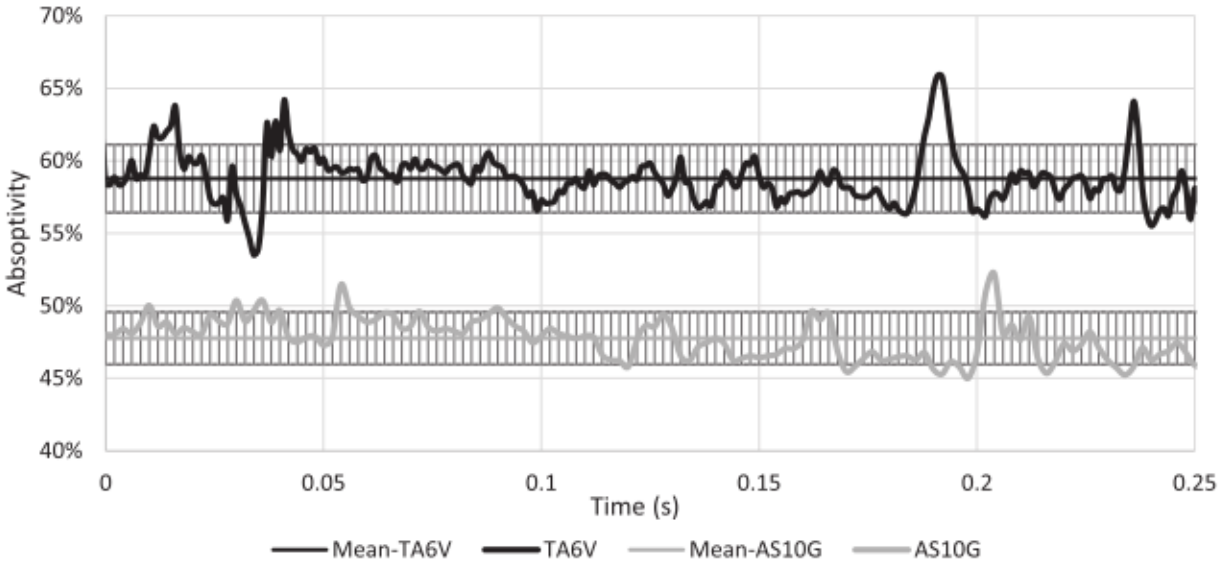

Fig. 12. Absorptivity of AS10G-48 μm and TA6V-45 μm with a powder layer in dynamic (spot 0,2 mm – thickness 100 μm).

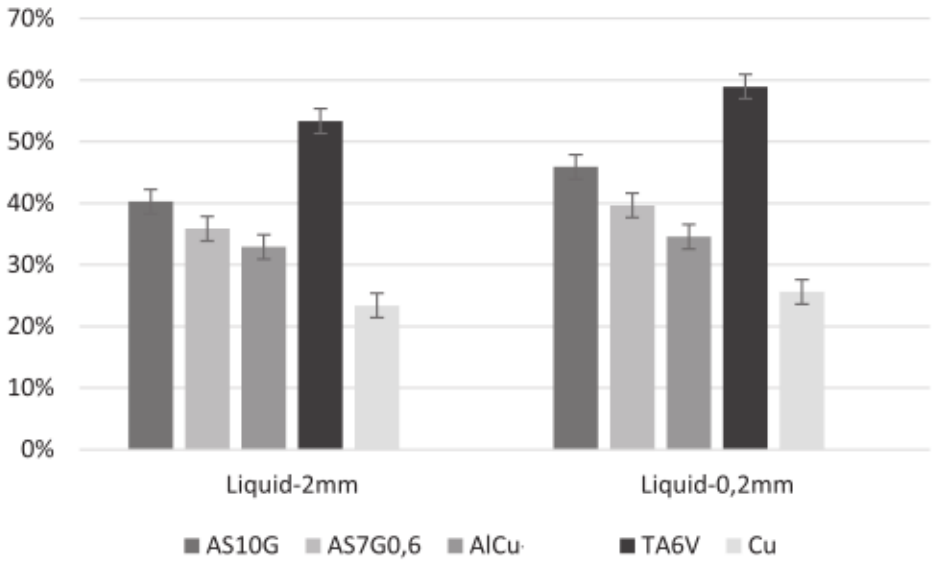

Fig. 13. Absorptivity for different bulk materials for a spot of 2 and 0.2 mm in liquid phase.

voids). Powder bed lay-up parameters such as thickness must be optimized for the material and the powder size and shape distribution. The temperature of the part can also have an impact on the attributed reflectivity measurement.

The paper studies the laser-powder interaction as the first step towards the liquid transition. A rapid transition has been observed due to the high energy deposition. Under the conditions of the SLM process, for example with a laser beam displacement of 2 m/s, it would take 10 μs to move the source 20 μm. The response time of the photodiode is about 1 ns in our study. It should therefore be possible to continuously evaluate the response of the laser/matter interaction during SLM. Indeed, in our study, the laser energy density has been divided by 800 compared to the LBM conditions (320 W-2 m/s). If we assume a linear response of the material, 80 ms can be considered for a laser power of 320 W and a laser spot of 0.2 mm. The liquid phase was indicated after 20 ms. It thus seems well representative of the laser/powder interaction. Furthermore, if the density filter is removed, the liquid phase time was observed at about 4 ms. A higher laser energy density was not studied with the small spot due to the limitation of the optical path structure used.

Sintering phenomena have been observed and have had an impact on the reflectivity. The proximity of the particles in this sintering phase makes the multi-diffusion more efficient. This state has been associated with a transition state to a liquid phase. Therefore, this transition could also be associated with the heat accumulated in the powder bed or with a contribution of both mechanisms. In the liquid phase, several hypotheses can be put forward: the conventional hypothesis according to which the laser beam directly strikes a continuous melt and the moving melt absorbs the free powder (Fig. 14 (a)) is used in the model of Xiao et al [20], while in the model of Gusarov et al [21] the laser beam interacts directly with the powder (Fig. 14 (b)). The first approach is correctly recognized and approved, for example, for laser cladding. However, the assumption of sudden consolidation is not obvious in the case of the SLM process because the process boundaries are very different. Indeed, the laser beam remains 1–2 orders of magnitude thinner and the coalescence time of two 100–150 μm particles measured experimentally was on the order of a few milliseconds to several tens of milliseconds [22] whereas the laser beam passage time is on the order of a fraction of a millisecond [23].

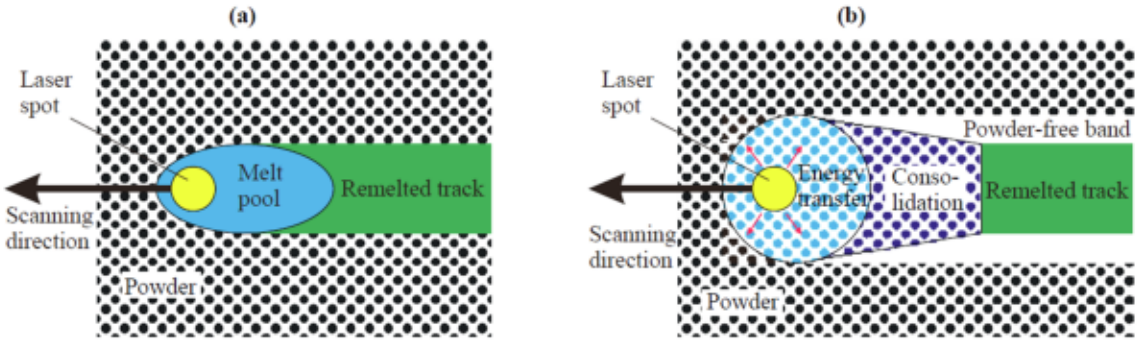

Fig. 14. Models of consolidation kinetics. Top view: (a) fast consolidation; (b) slow consolidation [20].

We have also observed the detachment of free powder in the melt resulting in the formation of powder-free bands on both sides of the remelted vector. This observation is interesting because the absorptance values could be used to identify the laser scanning parameters and especially to detect defects.

In powder bed laser fusion, three stages can be observed, track by track: initiation of laser interaction, steady state welding and quenching. At the beginning, there is a "true" laser-powder interaction until the laser-fluid interaction. At these interactions, it is also necessary to take into account the absorption rate of the substrate. However, the variation of the density of the powder bed associated with the roughness of the substrate and the granulometry of the powder can produce a deviation of the equilibrium which allows to have a continuous melt. This variation in density leads to a variation in reflectivity which can locally disturb the temperature gradient. The absorptivity under the melting conditions of the powder bed must therefore be evaluated and we have already observed a dynamic fluctuation during the laser-matter interaction.

Simonds et al [3] measure the dynamic absorbance of focused laser light incident on a spread metal powder surface, whose geometry is determined by XCT. This provides the pre-irradiated initial state of the spread powder, on which absorptance measurements are performed. These measurements reveal that the volume fraction of the particles changes significantly over the depth of interest (<100 μm) for light absorption. Similar results are shown in Figs. 8 and 9. Furthermore, by applying the results of a numerical model for absorptance, they highlight the importance of using time-dependent energy coupling values for validation of high-fidelity AM models to predict defects due to changes in melt behavior. To have predictive models, it is essential to know the dynamic absorption signatures as a function of the different regimes. This shows the necessity to have local information on the density of the powder bed for different melting regimes in order to adapt the laser power. For our study, the absorptivity was measured from the powder state to the liquid phase. It is complementary to the studies of Simonds et al [24] on the dynamic interaction state of the laser for the development of prediction tools for the AM process.

5. Conclusion

Laser absorption measurements were deduced using an experimental testbed operating an Ulbricht sphere. Several metallic materials were examined, associated with additive manufacturing applications. The laser-material interaction was more important for the powder than for the bulk material due to multi-scattering. The values obtained in this study can be used for the numerical simulation of the first instant of the laser-matter interaction. The layering of the powder bed is related to the powder particle size and layer thickness. The density of the powder bed and the illuminated surface were calculated for different configurations in terms of materials, powder thickness and powder distribution. We observed the evolution of the laser-material interaction and thus of the absorptivity over time, as the material changes from a solid state to a fluid state after a sintering phase.

Prospective studies are underway to investigate powder bed responses as a function of process parameters and strategies on a laboratory bench. It may be possible to evaluate the density of the powder bed layer by layer and to spatially compensate the energy density deposited by the laser (energy and/or velocity parameters). In-situ analysis combined with laser absorptivity measurements could be implemented to control the processes. However, further studies are needed.

Declaration of Competing Interest

The authors declare that they have no known competing financial interests or personal relationships that could have appeared to influence the work reported in this paper.

Data availability

No data was used for the research described in the article.

Acknowledgement

The authors gratefully acknowledge the ANR and industrial partners for financial assistance in the ANDDURO project.

References

[1] S.K. Everton, M. Hirsch, P. Stravroulakis, R.K. Leach, A.T. Clare, Review of in-situ process monitoring and in-situ metrology for metal additive manufacturing, Mater. Des. 95 (2016) 431–445.
[2] D. Koutny, D. Palousek, L. Pantelejev, C. Höller, R. Pichler, L. Tesicky, J. Kaiser, Influence of scanning strategies on processing of aluminum alloy EN AW 2618 using selective laser melting, Materials 11 (2) (2018) 298–316.
[3] B.J. Simonds, E.J. Garboczi, T.A. Palmer, P.A. Williams, Dynamic laser absorptance measured in a geometrically characterized stainless-steel powder layer, Phys. Rev. Appl 13 (2020), 024057.
[4] C.D. Boley, S.A. Khairallah, A.M. Rubenchik, Calculation of laser absorption by metal powders in additive manufacturing, Appl. Opt 54 (9) (2015) 2477–2482.
[5] M. Gürtler, K. Karg, H. Leitz, M. Schmidt, Simulation of laser beam melting of steel powders using the three-dimensional volume of fluid method, Phys. Procedia 41 (2013) 881–886.
[6] US. Bertoli, G. Guss, S. Wu, M. J. Matthews b, J. M. Schoenung, In-situ characterization of laser-powder interaction and cooling rates through high-speed imaging of powder bed fusion additive manufacturing, Mater. Des. 35 (2017) 385-396.
[7] L. Haferkamp, A. Spierings, M. Rusch, D. Jermann, M.A. Spurek, K. Wegener, Effect of Particle size of monomodal 316L powder on powder layer density in powder bed fusion, Progr. Additive Manuf. 6 (2021) 367–374.
[8] N.K. Tolochko, Y.V. Khlopkov, S.E. Mozzharov, M.B. Ignatiev, T. Laoui, V.I. Titov, Absorptance of Powder Materials Suitable for Laser Sintering, Rapid Prototyping J. 6 (3) (2000) 155–161.
[9] T. Furumoto, T. Ueda, A. Hosokawa, S. Abe, T.H.C. Childs, Study on the Measurement of Physical Properties in the Metal Powder for Rapid Prototyping, J. Japan Soc. Precis. Eng. 73 (2007) 558–562.
[10] A.V. Gusarov, J.-P. Kruth, Modelling of Radiation Transfer in Metallic Powders at Laser Treatment, Int. J. Heat Mass Transfer 48 (2005) 3423–3434.
[11] U. Ali, Y. Mahmoodkhani, S.I. Shahabad, R. Esmaeilizadeh, F. Liravi, E. Sheydaeian, K.Y. Huang, E. Marzbanrad, M. Vlasea, E. Toyserkani, On the measurement of relative powder-bed compaction density in powder-bed additive manufacturing processes, Mater. Des. 155 (2018) 495–501.

[12] J.W. Carson, B.H. Pittenger, Bulk Properties of Powders, Powder Metal Technologies and Applications, ASM Handbook 7 (1998) 287–301.
[13] R. Kromer, J. Cormier, S. Costil, Role of powder granulometry and substrate topography in adhesion strength of thermal spray coatings, J. Therm. Spray Technol. 25 (5) (2016) 933–945.
[14] H.W. Mindt, M. Megahed, N.P. Lavery, M.A.J. Holmes, S.G.R. Brown, Powder bed layer characteristics: the overseen first-Order process input, Metall. Mater. Trans. A 47 (8) (2016) 3811–3822.
[15] G. Jacob, A. Donmez, J. Slotwinski, S. Moylan, Measurement of powder bed density in powder bed fusion additive manufacturing processes, Meas. Sci. Technol. 27 (2016) 115601.
[16] D. Bergstrom, The Absorption of Laser Light by Rough Metal Surfaces -, Lulea University of Technology, 2008. PhD Thesis.
[17] C.D. Boley, S.D. Mitchell, A.M. Rubenchik, et al., Metal powder absorptivity: modeling and experiment, Appl. Opt. 55 (23) (2016) 6496–6501.
[18] H.C. Chen, G. Bi, M.L.S. Nai, Enhanced welding efficiency in laser welding of highly reflective pure copper, J. Mater. Process. Technol. 216 (2015) 287–293.
[19] V. Gunenthiram, P. Peyre, M. Schneider, M. Dal, F. Coste, R. Fabbro, Analysis of laser melt pool powder bed interaction during the selective laser melting of a stainless steel, J. Laser Appl. 29 (2017) 022303.
[20] B. Xiao, Y. Zhang, Numerical Simulation of Direct Metal Laser Sintering of Single-Component Powder on Top of Sintered Layers, J. Manuf. Sci. Engineering, 130 (2008) (041002).
[21] I. Gusarov, P.h. Yadroitsev, P.h. Bertrand, I. Smurov, Heat transfer modelling and stability analysis of selective laser melting, Appl. Surf. Sci. 254 (4) (2007) 975–979.
[22] F. Klocke, C. Wagner, Coalescence behaviour of two metallic particles as base mechanism of selective laser sintering, CIRP Ann. 52 (2003) 177.
[23] I. Yadroitsev, I. Smurov, Selective laser melting technology: From the single laser melted track stability to 3D parts of complex shape, Phys. Procedia 5 (B) (2010) 551–560.
[24] B.J. Simonds, J. Tanner, A. Artusio-Glimpse, E.J. Garboczi, P.A. Williams, N. Parab, C. Zhao, T. Sun, The causal relationship between melt pool geometry and energy absorption measured in real time during laser-based manufacturing, Appl. Mater. Today 23 (2021), 101049.